JOC*Article*

Rearrangement Pathways of Five-Membered Ring Enlargement in Carbocations: Quantum Chemical Calculations and Deuterium Kinetic Isotope Effects

Valerije Vrček,[†] Martin Saunders,[‡] and Olga Kronja*[,†]

Faculty of Pharmacy and Biochemistry, University of Zagreb, A. Kovačića 1, P.O. Box 156, 10000 Zagreb, Croatia, and Department of Chemistry, Yale University, New Haven, Connecticut 06520

kronja@pharma.hr

Received November 13, 2002

Three plausible routes for the five-membered ring expansion in the equilibrating 2-cyclopentyl-2-propyl and 1-(2-propyl)cyclopentyl cations **1A**/**1B** were located on the PES, all calculated at the MP4/6-31G(d)//MP2/6-31G(d) level of theory. In pathway I, the six-membered transition structure (**TS-I**) connects the less stable cyclopentyl cation **1A** and the 1,2-dimethylcyclohexyl carbocation (**2**) via a barrier of 16.4 kcal/mol. In pathway II, which has a barrier of 16.3 kcal/mol, the methyl migration occurs first in the more stable **1B** via transition structure **TS-II**. Pathway III involves the uphill hydride shift and formation of the secondary cation **3**, which undergoes Wagner−Meerwein 1,2-isopropyl shift via a transition structure **TS-III** and the protonated carbocation intermediate **4**. The barrier pathway III is for 17.0 kcal/mol. Experimental secondary deuterium isotope effects of the rearrangement were measured for the hexadeuterated **1A-d$_6$**/**1B-d$_6$** (k_H/k_D = 2.40) and tetradeuterated **1A-d$_4$**/**1B-d$_4$** (k_H/k_D = 0.18) cations by means of ^{1}H NMR. Comparison of the experimental data with the theoretical values (k_H/k_D = 2.40 for **1B-d$_6$** and k_H/k_D = 0.24 for **1B-d$_4$**, respectively) obtained with QUIVER revealed that pathway II is a major reaction route.

Introduction

In the biogenesis of steroids and triterpenoids, an important step is the expansion of the five-membered rings of carbocation intermediates to six-membered rings.[1] For example, the enzymatic cyclization of 2,3-epoxysqualene in animals proceeds through a tricyclic carbocation in which the C ring is five-membered.[2] Enlargement of the C ring is accompanied by a simultaneous or subsequent methyl migration and formation of the D ring and leads to the protosteryl cation (Scheme 1), which is a common intermediate for all steroid hormones. Expansion of a five-membered ring was also suggested in biosynthesis of phytosterols in numerous cases. For example, the lupenyl cation undergoes ring enlargement process yielding oleanyl and taraxasteryl cations (Scheme 1).[3]

To get more insight into the ring-expansion process, we chose to investigate it using model carbocations. As shown with the darkened bonds in Scheme 1, the simplest model is the 2-cyclopentyl-2-propyl cation (**1A**).

The model cation is not static in superacid solution, but undergoes rapid nondegenerate hydride shifts, interchanging the 2-cyclopentyl-2-propyl cation **1A** and the 1-(2-propyl)cyclopentyl cation **1B**.[4] The temperature-dependent ^{13}C shifts and the relative shielding of the carbons showed that the equilibrium favors the isomer **1B**. The enthalpy of $\Delta H^{\ddagger} = -1.4$ kcal/mol and the entropy of $\Delta S^{\ddagger} = 3.5$ cal/K mol were obtained for the intercon-

SCHEME 1

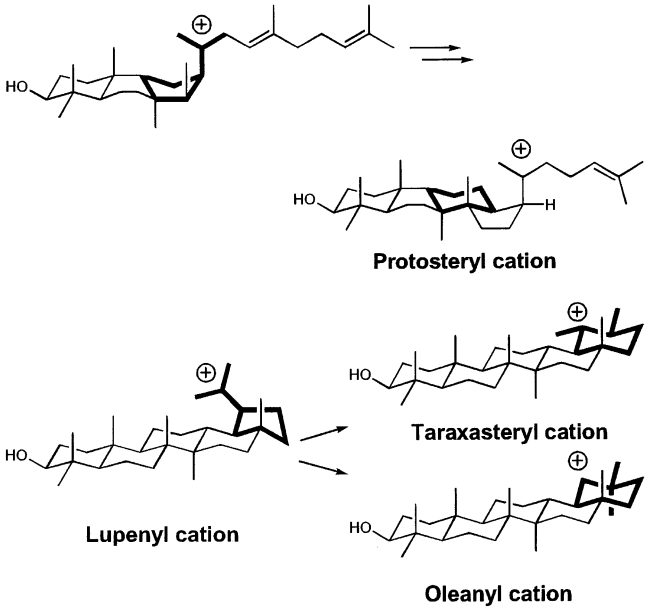

* To whom correspondence should be addressed. Phone: +385 1 481 8301. Fax: +385 1 485 6201. E-mail (alternate): kronja@rudjer.irb.hr.
[†] University of Zagreb.
[‡] Yale University.

(1) (a) Abe, I.; Rohmer, M.; Prestwich, G. D. *Chem. Rev.* **1993**, *93*, 2189. (b) Wendt, K. U.; Schulz, G. E.; Corey, E. J.; Liu, D. R. *Angew. Chem., Int. Ed.* **2000**, *39*, 2812.

(2) Corey, E. J.; Virgil, S. C.; Cheng, H.; Baker, C. H.; Matsuda, S. P. T.; Singh, V.; Sarshar, S. *J. Am. Chem. Soc.* **1995**, *117*, 11819.

(3) Seo, S.; Yoshimura, Y.; Uomori, A.; Takeda, K.; Seto, H.; Ebizuka, Y.; Sankawa, U. *J. Am. Chem. Soc.* **1988**, *100*, 1740.

(4) Siehl, H.-U.; Vrcek, V.; Kronja O. *J. Chem. Soc., Perkin Trans. 2* **2002**, 106.

10.1021/jo020694p CCC: $25.00
Published on Web 01/31/2003

TABLE 1. Total and Relative Energies for Carbocations Involved in Pathways I, II and III

	E/hartree		Δ*E*/kcal mol^{-1}		*E*/hartree	
cation	B3LYP/6-31G(d) (ZPE)[a] [NImag; ν, cm^{-1}][b]	MP2/6-31G(d) (ZPE) [NImag; ν, cm^{-1}]	B3LYP/6-31G(d) + ZPE	MP2/6-31G(d) + ZPE	MP4/6-31G(d)//MP2/ 6-31G(d) (ZPE)[c]	Δ*E*/kcal mol^{-1}
1A	−313.610958 (0.213313) [0]	−312.451585 (0.218267) [0]	1.60	0	−312.573233 (0.218267)	0.5
1B	−313.612480 (0.212465) [0]	−312.448807 (0.216891) [0]	0	0.6	−312.572712 (0.216891)	0
TS−I	−313.584583 (0.212556) [1; −277]	−312.422671 (0.217017) [1; −347]	17.7	17.4	−312.546671 (0.217017)	16.4
TS−II	−313.585029 (0.212330) [1; −144]	−312.422992 (0.216664) [1; −170]	17.1	16.9	−312.546490 (0.216664)	16.3
TS−III		−312.427333 (0.218660) [1; −38]		15.5	−312.547367 (0.218660)	17.0
3TS	−313.589487 (0.213519) [1; −49]	−312.423835 (0.216156) [1; −52]	14.6	16.1	−312.548919 (0.216156)	14.4
3	−313.589487 (0.213519) [0]	−312.432743 (0.218614) [0]	15.1	12.0	−312.554007 (0.218614)	12.8
4	−313.582468 (0.213684) [1; −77]	−312.427452 (0.217594) [0]	19.5	14.7	−312.549244 (0.217594)	15.2
4TS	−313.581928 (0.212498) [1; −475]	−312.428752 (0.219107) [1; −411]	19.2	14.9	−312.548214 (0.219107)	16.8
2[d]	−313.618724 (0.214062) [0]	−312.456948 (0.218362) [0]	−2.9	−3.3	−312.580283 (0. 218362)	−3.8
2TS	−313.598719 (0.211446) [1; −469]	−312.438777 (0.216173) [1; −64]	7.9	6.7	−312.561368 (0. 216173)	6.6

[a] Zero-point vibrational energy obtained from frequency calculation. [b] Number of imaginary frequencies obtained from frequency calculation. [c] ZPE corrections calculated at the MP2/6-31G(d) level. [d] Data for the most stable isomer.

version **1A** → **1B**. The limits of the barrier for hydride migration at −127 °C were set to $5.0 < \Delta G^{\ddagger} < 5.2$ kcal/mol. Quantum chemical calculations carried out for model structures **1A** and **1B** at B3LYP/6-31G(d) and MP4/6-31G(d)//MP2/6-31G(d) levels of theory agree with the observation that the positive charge prefers to be located on the endocyclic carbon.

We showed in our preliminary investigation that at about −100 °C a ring-enlargement process and formation of the 1,2-dimethyl-1-cyclohexyl cation (**2**) occurred.[5] The rearranged cation **2** undergoes a rapid degenerate hydride shift over a low barrier ($\Delta G^{\ddagger} = 3.7$ kcal/mol at −136 °C).[6] From the first-order rate constant for the conversion **1A**/**1B** → **2**, the free energy of activation of the ring enlargement process of $\Delta G^{\ddagger}$ (99 °C) = 12.0 kcal/mol was found. The similar barrier (12.3 kcal/mol) was calculated at the B3LYP/6-31G(d)//HF/6-31G(d) level for the ring-enlargement process of the tertiary 2-(2,2,3-pentamethylcyclopentyl)-2-propyl cation to the secondary 1,1,2,2,3-pentamethyl-6-cyclohexyl cation.[7]

Solutions of the stable ions **1A**/**1B** undergo expansion of the five-membered ring as indicated by ^{1}H and ^{13}C NMR spectroscopy, demonstrating the suitability of **1A**/**1B** as a model system for investigation of the mechanism of biomimetic ring expansion. We have now carried out quantum chemical calculations with **1A**/**1B** in order to explore the possible reaction routes and also kinetic measurements with the protio and deuterated isotopomers of **1A**/**1B** to get experimental evidence concerning the reaction mechanism.

Results and Discussion

We suggest three possible mechanisms for the ring expansion of the cation **1A**/**1B**, as shown in Scheme 2. According to pathway I, the first step of the rearrangement is the ring expansion of the less stable isomer **1A** and the formation of the secondary ion intermediate or transition state, followed by 1,2-methyl migration. In pathway II, the rearrangement starts with the more stable isomer **1B**. Prior to the ring expansion, an uphill methyl migration occurs, yielding the secondary ion intermediate or transition state. Sigmatropic shift of the C1−C2 endocyclic bond leads to the formation of the cation **2**.

Pathway III involves an uphill hydride shift forming the secondary cation **3**, which undergoes Wagner−Meerwein 1,2-isopropyl shift via a protonated carbocation intermediate **4**. Corner-to-corner hydride shift, with consecutive or simultaneous C1−C2 bond cleavage, could lead to **2**.

Theoretical Results. The quantum chemical calculations were performed using Gaussian94.[8] The energies

(5) Vrcek, V.; Siehl, H.-U.; Kronja, O. *J. Phys. Org. Chem.* **2000**, *13*, 616.
(6) Saunders: M.; Kates, M. R. *J. Am. Chem. Soc.* **1978**, *100*, 7082.
(7) Jenson, C.; Jorgensen, W. L. *J. Am. Chem. Soc.* **1997**, *119*, 10846.

SCHEME 2

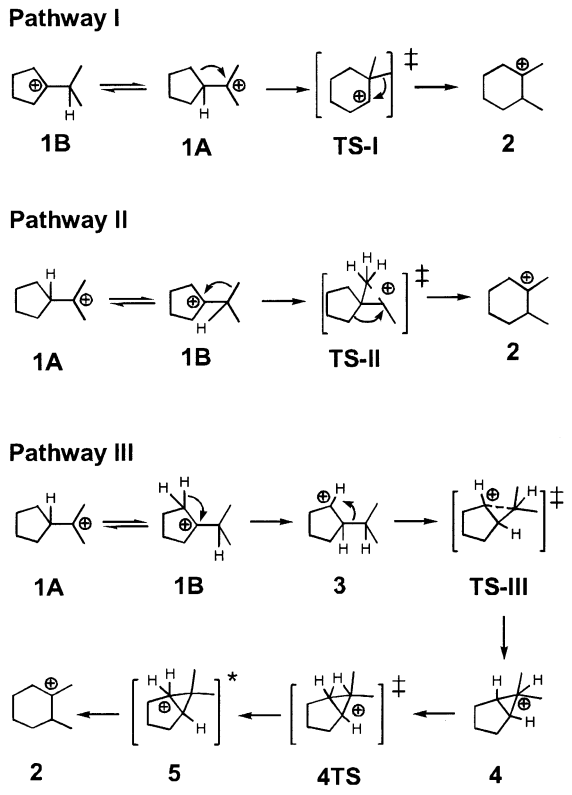

of the minimum and transition structures are given in Table 1. The relative energies with respect to **1B** are given in Table 1 and in Figure 1. The structures of the rate-determining transition states (**TS-I**, **TS-II**, and **TS-III**) along with a key geometry parameters are given in Figure 2. The energy minimum and transition structures, not previously described, are given in Figure 3.

Theoretical results for pathway I showed that the six-membered transition state (**TS-I**) connects the cyclopentyl cation **1A** and the 1,2-dimethylcyclohexyl carbocation (**2**). At the MP4/6-31G(d)//MP2/6-31G(d) level, the transition structure **TS-I** is 16.4 kcal/mol less stable than the cyclopentyl structure **1B**. The transition structure **TS-I** adopts a boat conformation (Figure 2) and is characterized by elongated C1−C5 (2.39 Å) and C1′−C5 distances (1.63 Å) and the slight shift of the axial methyl group toward C5 carbon atom. The only imaginary vibration frequency (347*i* cm^{-1}) is associated with the elongation of the endocyclic C1−C5 bond and the simultaneous formation of the C1′−C5 bond, which is consistent with the ring-expansion process.

Calculations for pathway II revealed that the rearrangement proceeds via transition structure **TS-II**, which connects cyclopentyl cation **1A** and 1,2-dimethyl cyclohexyl cation **2**. **TS-II** is a methyl bridged structure (Figure 2) characterized by elongated C1−C2′ and C1′−C2′ distances (1.58 and 2.36 Å, respectively) and relatively small bridging angle (C1−C2′−C1′ is 36°). The imaginary frequency (170*i* cm^{-1}) corresponds to the methyl group migration and simultaneous sigmatropic shift of the endocyclic C1−C5 bond. The calculated energy barrier for this process at the MP4/6-31G(d)//MP2/6-31G(d) level is 16.3 kcal/mol.

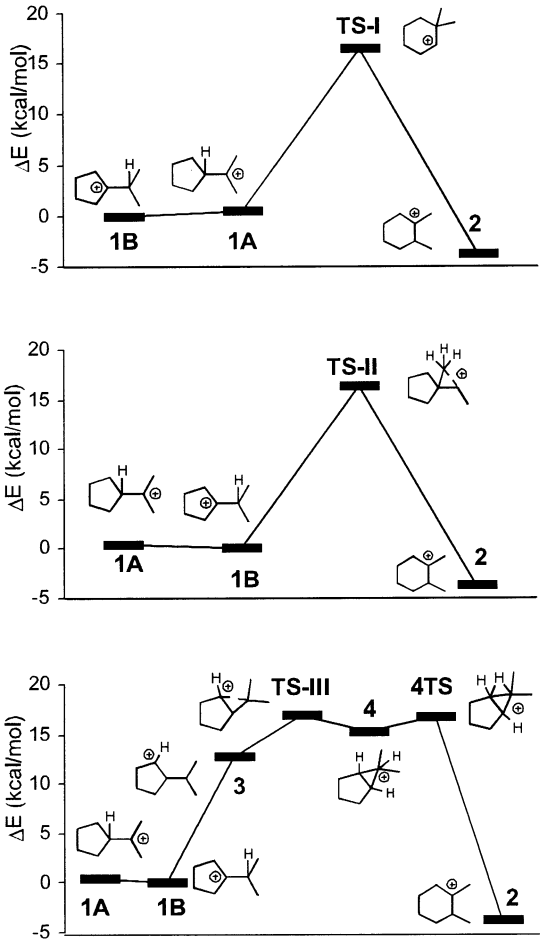

FIGURE 1. Reaction energy profiles for the ring expansion pathways I, II, and III calculated at the MP4/6-31G(d)//MP2/6-31G(d) level of theory.

The third possible mechanism for the ring-expansion process (pathway III) involves the three energy minimum structures (**1B**, **3**, and **4**) separated by two barriers. The secondary carbocation **3** (Figure 3) is formed by uphill 1,2-hydride migration through the hydrido-bridged transition structure **3TS** that connects the high-energy secondary intermediate **3** and cyclopentyl cation **1B**. In cation **3**, the C1−C1′ bond is elongated (1.739 Å) and the C1′−C1−C2 angle is reduced (78.4°), suggesting hyperconjugative stabilization of the positive charge. The calculated energy barrier for the uphill 1,2-hydride shift is 14.4 kcal/mol at the MP4/6-31G(d)//MP2/6-31G(d) level of theory.

The secondary carbocation **3** undergoes a 1,2-isopropyl shift to give a protonated carbocation intermediate **4** (Figure 3). At the B3LYP/6-31G(d) level, the symmetrical (C_s point group) structure **4** was located as a transition structure, while at the MP2/6-31G(d) level, **4** is an energy minimum structure which is 3.7 kcal/mol less stable than the secondary carbocation intermediate **3**. The highest

(8) Frisch, M. J.; Trucks, G. W.; Schlegel, H. B.; Gill, P. M. W.; Johnson, B. G.; Robb, M. A.; Cheeseman, J. R.; Keith, T.; Petersson, G. A.; Montgomery, J. A.; Raghavachari, K.; Al-Laham, M. A.; Zakrzewski, V. G.; Ortiz, J. V.; Foresman, J. B.; Cioslowski, J.; Stefanov, B. B.; Nanayakkara, A.; Challacombe, M.; Peng, C. Y.; Ayala, P. Y.; Chen, W.; Wong, M. W.; Andres, J. L.; Replogle, E. S.; Gomperts, R.; Martin, R. L.; Fox, D. J.; Binkley, J. S.; Defrees, D. J.; Baker, J.; Stewart, J. P.; Head-Gordon, M.; Gonzalez, C.; Pople, J. A. *Gaussian 94*, revision E.1; Gaussian, Inc.: Pittsburgh, PA, 1995.

stationary point at the PES of pathway III at the MP4/6-31G(d)//MP2/6-31G(d) level is the transition structure **TS-III** which connects intermediates **3** and **4** (Table 1). The calculated energy barrier for the overall ring expansion (pathway III) via the transition structure **TS-III** is 17.0 kcal/mol. According to the quantum chemical results, the structure **5** that could be obtained via corner-to-corner 1,2-hydride shift is not an energy minimum. Instead, cation **4** gives rearranged product **2** directly through transition structures **4TS**. At the MP4/6-31G(d)//MP2/6-31G(d) level, **4TS** is 16.8 kcal/mol less stable than **1B**.

Finally, it should be mentioned that six energy minimum structures for the product, 1,2-dimethylcyclohexyl cation **2**, were located on the PES, four having chair structures[5] and two conformers assuming boat structures. Fast degenerate 1,2-hydride shifts interchange these six isomers through the symmetrical (C_s point group) hydrido-bridged transition structure **2TS** having a boat structure.

Computational simulations of the rearrangement processes suggest (Table 1) that all three pathways are plausible since all proceed through barriers that are similar in energy. Pathway III goes through the transition structure **TS-III** and is 0.6 kcal/mol less favorable than the corresponding process via the transition structure **TS-I** (pathway I) and 0.7 kcal/mol less favorable than the process which involves the transition structure **TS-II** (pathway II).

***β*-Deuterium Kinetic Isotope Effects.** To decide among the three possible mechanisms, we measured the rearrangement rates (k_{obs}) of the hexadeuterated and tetradeuterated model cations, **1A-d$_6$**/**1B-d$_6$** and **1A-d$_4$**/**1B-d$_4$**, respectively, and calculated the secondary deuterium kinetic isotope effects (KIE).[9] The cations were prepared from the corresponding deuterated alcohols by molecular beam method in $SbF_5/SO_2F_2-SO_2ClF$.[10] The rate of the rearrangement was followed by means of ^{1}H NMR spectroscopy described in detail in the Methods.

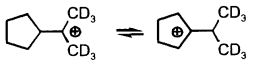

1A-d$_6$ **1B-d$_6$**

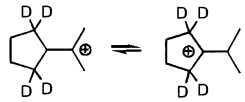

1A-d$_4$ **1B-d$_4$**

The first-order reaction rates (k_{obs}) for the protio isotopomers at three different temperatures, as well as for the hexadeuterated (**1A-d$_6$**/**1B-d$_6$**) and tetradeuterated (**1A-d$_4$**/**1B-d$_4$**) isomers, respectively, are presented in Table 2. The observed reaction rate (k_{obs}) is determined together with the rearrangement rate (k_r) and the fraction (x) of the starting carbocation. The fractions of isomers **1A** and **1B** at a given temperature, which depend on the equilibrium constant for interconversion **1A**/**1B**, are given with the following equations:

$$x_{1A} = \frac{1}{K_{eq} + 1} \qquad x_{1B} = \frac{K_{eq}}{K_{eq} + 1}$$

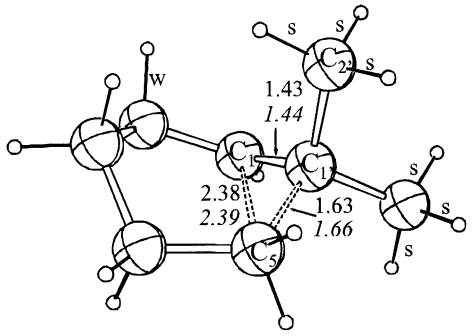

TS-I

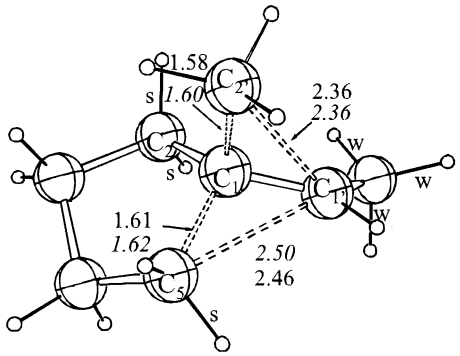

TS-II

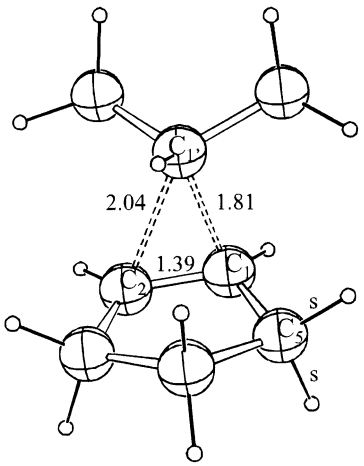

TS-III

FIGURE 2. MP2/6-31G(d)-optimized rate-determining transition structures **TS-I**, **TS-II**, and **TS-III** for pathways I, II, and III, respectively. Bond lengths are in angstroms (B3LYP/6-31G(d) optimized values in italics). C−H bonds marked as "w" or "s" are weaker or stiffer, respectively, than the corresponding bonds in the ground state.

(9) For general treatment of isotope effects, see: (a) Biegeleisen, J.; Wolfsberg, M. *Adv. Chem. Phys.* **1958**, *1*, 15. (b) Melander, L. *Isotope Effects on Reaction Rates*; Ronald Press: New York, 1960. (c) Collins, C. I., Bowman N. S., Eds. *Isotope Effects in Chemical Reactions*; ACS Monograph 167; Van Norstand Reinhold: New York, 1970. (d) Wolfsberg, M. *Acc. Chem. Res.* **1972**, *7*, 225. (e) Melander, L.; Saunders, W. H., Jr. *Reaction Rates of Isotopic Molecules*; Wiley: New York, 1980.

(10) Saunders, M.; Vogel, P. *J. Am. Chem. Soc.* **1971**, *93*, 2559.

TABLE 2. Observed Reaction Rates of the Rearrangement 1A/1B → 2, Preequilibrium Constants, and Calculated Rates of the Rearrangements 1A → 2 and 1B → 2

compd	*T*/°C	$k_{obs}/10^{-4}$ s^{-1}	K_{eq}[a,b]	k_r (**1A→2**)$/10^{-4}$ s^{-1}	k_r (**1B→2**)$/10^{-4}$ s^{-1}
1A/1B	−109	1.00 ± 0.07	12.5	13.5 ± 0.95	1.08 ± 0.08
	−103	2.46 ± 0.15	11.2	30.0 ± 1.83	2.70 ± 0.16
	−92	12.2 ± 0.87	8.1	111.0 ± 7.92	13.7 ± 0.98
	−96			70.2 ± 4.37	7.8 ± 0.47[c]
1A-d$_6$/1B-d$_6$	−92	5.42 ± 0.44	18.4	105.1 ± 8.54	5.7 ± 0.46
1A-d$_4$/1B-d$_4$	−96	28.9 ± 0.75	1.9	83.8 ± 2.17	43.9 ± 1.14

[a] K_{eq} = [**1B**]/[**1A**]. [b] Reference 4. [c] Extrapolated value.

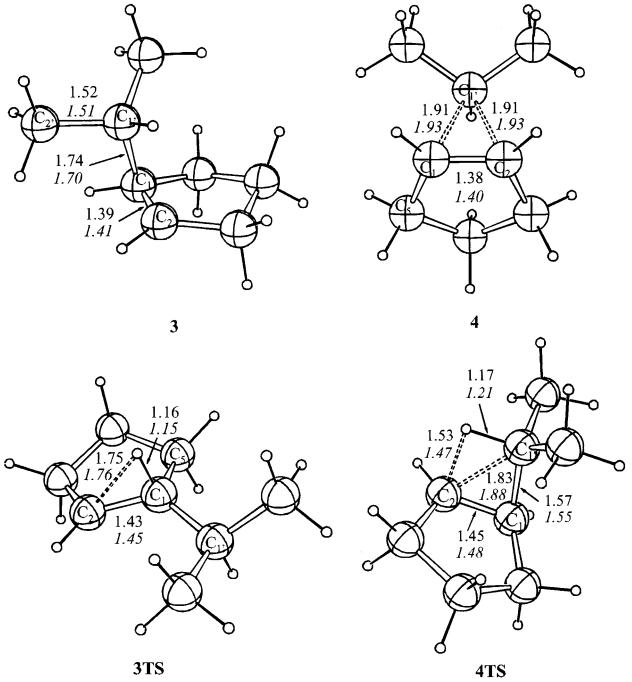

FIGURE 3. MP2/6-31G(d)-optimized high-energy intermediates **3** and **4** and transition structures **3TS** and **4TS** involved in pathway III. Bond lengths in angstroms (B3LYP/6-31G(d) optimized values in italics).

The equilibrium constants for protio and deuterated cations**,** calculated earlier from the experimental and calculated chemical shifts,[4,11] are presented in Table 2.

If the rearrangement starts from **1A** (**1A → 2**), as is the case in pathway I, the rearrangement rate ($k_{r(1A→2)}$) is equal to the ratio of the observed reaction rate to the fraction of isomer **1A** at given temperature, while if the rearrangement starts from **1B** (**1B → 2**), as is the case with pathways II and III, the rearrangement rate ($k_{r(1B→2)}$) is equal to the ratio of the observed reaction rate to the fraction of isomer **1B**.

$$k_{r(1A→2)} = \frac{k_{obs}}{x_{1A}} \qquad k_{r(1B→2)} = \frac{k_{obs}}{x_{1B}}$$

The rearrangement rates for both processes, **1A → 2** and **1B → 2**, respectively, are presented in also in Table 2.

Since two sets of rearrangement rates were obtained, depending on whether the rearrangement starts from the **1A** or **1B** isomer, we also calculated two sets of activation parameters. For the possible **1A → 2** process, $\Delta H^{\ddagger} = -29.2 \pm 0.1$ and $\Delta S^{\ddagger} = -117 \pm 7.6$, respectively, while for the possible **1B → 2** process $\Delta H^{\ddagger} = -35.6 \pm 0.1$ and $\Delta S^{\ddagger} = -99.1 \pm 3.5$ were obtained. These values are consistent with all three proposed mechanisms in which the high degree of order, which is required in the transition state (unfavorable changes in $\Delta S^{\ddagger}$) is overcompensated with rather small $\Delta H^{\ddagger}$.

TABLE 3. Theoretical Secondary Deuterium KIEs (k_H/k_D) for Three Possible Pathways and the Experimental Secondary Deuterium KIEs of the Rearrangements 1A → 2 and 1B → 2

method	mechanism	**1A-d$_6$/1B-d$_6$**[a]	**1A-d$_4$/1B-d$_4$**[b]
calculated (QUIVER)[c]	pathway I	0.59	1.88 (1.72)[c]
	pathway II	**2.24**	**0.24 (0.32)**
	pathway III	0.89	0.29 (0.34)
experimental	**1A → 2**	1.06 ± 0.11	0.83 ± 0.06
	1B → 2	**2.40** ± 0.26	**0.18** ± 0.01

[a] At −92 °C; [b] At −96 °C; [c] If complete deuterium scrambling is included; the force constant matrix obtained at MP2/6-31G(d) level was used as in input to QUIVER.

KIEs are the ratios of the rearrangement rates of the protio and deuterated compounds ($k_{r(H)}/k_{r(D)}$). Again we also calculated two sets of experimental deuterium KIEs depending whether the rearrangement starts from **1A** or **1B** isomer. The results are presented in Table 3.

If one can locate the starting structure and the transition state for a reaction using theoretical calculations, one can employ the program QUIVER,[12] putting in the isotopes in the correct places, and get a theoretically predicted KIE. Since we located the energy minimum structures **1A** and **1B** [4] and transition structures **TS-I**, **TS-II**, and **TS-III** for possible pathways I, II, and III, we were able to calculate the KIEs for the hexadeuterated and tetradeuterated isomers using the force constant matrix obtained at the MP2/6-31G(d) level of theory as an input. Theoretical KIEs for all three possible mechanisms are given in Table 3.

To decide among the possible mechansims, theoretical KIEs for pathway I are compared with experimental values based on rearrangement that starts form **1A** isomer (**1A → 2**), and the theoretical KIEs obtained for pathways II and III are compared with the experimental values based on rearrangement that starts from **1B** isomer (**1B → 2**).

The experimental KIEs for process **1A → 2** are opposite to those predicted theoretically for pathway I; therefore, pathway I can be ruled out as a major reaction route. The results presented in Table 3 reveal excellent agree-

(11) Vrcek, V.; Kronja, O.; Siehl, H.-U. *J. Chem. Soc., Perkin Trans. 2* **1999**, 1317.

(12) Saunders, M.; Laidig, K. E.; Wolfsberg, M. *J. Am. Chem. Soc.* **1989**, *111*, 8989.

SCHEME 3

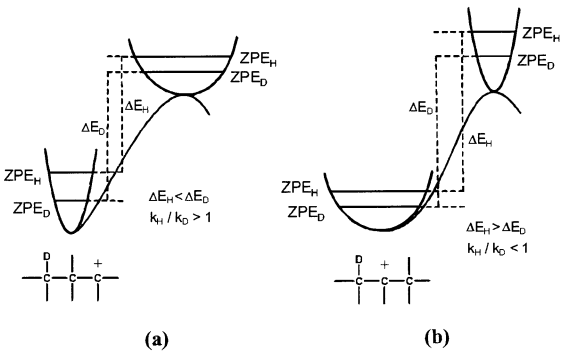

ment between the experimental KIEs for process **1B** → **2** for both the hexadeuterated and tetradeuterated isomers and the theoretical KIEs predicted for pathway II, so pathway II can represent the major reaction pathway. In comparison with the theoretically predicted KIEs for pathway III and the experimental KIEs for process **1B** → **2**, only the results for the tetradeuterated isotopomer are in accord, while KIEs obtained for the hexadeuterated isomer are inconsistent. Due to that discrepancy, pathway III can be also ruled out as a major reaction pathway.

The calculated KIEs can be rationalized if the vibration frequencies of some C−H(D) bonds are considered in detail. According to chosen pathway II, the starting compound is **1B**, in which all methyl C−H bonds length and bond angels have usual values. However, in the transition structure **TS-II** the same C−H bonds, marked as "w" ("weaker") in Figure 2, are elongated and the corresponding bond angles are reduced. Weakening of the methyl C−H bonds is due to their involvement in the hyperconjugative stabilization of the positive charge generated on C1′ in the transition state. If those hydrogens are replaced with deuteriums, as is the case in **1B-d$_6$**, the zero-point vibration frequency of the deuterated compound is lowered more in the starting cation **1B-d$_6$** than in the transition state **TS-I-d$_6$**, as presented in Scheme 3a. Thus, the vibration energy difference between the ground and transition state for the deuterated compound is larger than for the protio compound (Scheme 3a). Therefore, the deuterated compound rearranges more slowly than the protio isomer (experimental $k_H/k_D = 2.4$).

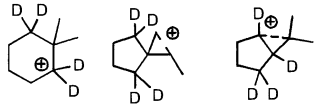

TS-I-d$_4$ **TS-II-d$_4$** **TS-III-d$_4$**

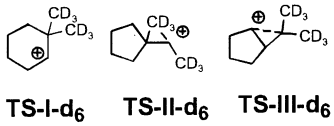

TS-I-d$_6$ **TS-II-d$_6$** **TS-III-d$_6$**

The methylene C−H bonds at C2 and C5 take part in stabilizing of the positive charge in the starting compound **1B**. Those bonds are longer and less stiff, and the corresponding bond angles are reduced. In the transition structure **TS-II**, however, these bonds, marked as "s" ("stiffer") in Figure 2, become shorter and stiffer, since the positive charge is formally moved to next carbon atom. If those hydrogens are replaced with deuteriums as in **1B-d$_4$**, the zero-point vibration frequency of the deuterated compound is lowered less in the starting cation than in the transition state, as presented in Scheme 3b. The vibration energy difference between the ground and transition states for the deuterated compound becomes larger than for the protio compound, and the rearrangement of the protio isotopomer is slower than for the deuterated compound, i.e., inverse KIE occurs ($k_H/k_D = 0.18$).

On the basis of considerations similar to those above, the theoretical KIEs for pathway I can be easily verified and the mechanism ruled out. Due to hyperconjugation, the methyl C−H bonds (marked as "s") in the starting cation **1A** are less stiff than in the transition structure **TS-I**. These hydrogens are replaced with deuteriums in hexadeuterated compound **1A-d$_6$**. Therefore, if pathway I were operative, the hexadeuterated compound would rearrange considerably slower than the protio analogue, as predicted theoretically (Table 3). On the contrary, the C−H bonds (marked as "w") involved in hyperconjugative stabilization of the positive charge **TS-I** are replaced with C−D bonds in the tetradeuterated compound (**1A-d$_4$**), so unlike the inverse experimental KIE, the protio compound would rearranged faster than the tetradeuterated isomer. Even though the predicted KIEs for pathway I are the opposite of those obtained, because of the almost same barrier calculated, one cannot rule out that a fraction of the reaction proceed through this rout. Since only a small fraction of cation **1A** exists in the starting mixture, the net KIEs would be affected only slightly.

To verify the theoretical KIEs for pathway III, we examined the methyl C−H bonds in the starting structure **1B-d$_6$** and in the rate determining **TS-III**. We found that neither of these bond lengths or bond angels are changed considerably. That explains the theoretical KIE of the hexadeuterated isomers, which is close to unity ($k_H/k_D = 0.89$). Relatively large KIE obtained experimentally clearly rule out this route as a major reaction ($k_H/k_D = 2.4$).

The hydride shift process **1A** → **3** in pathway III (Scheme 2) is feasible since the corresponding energy barrier is relatively small (14.4 kcal/mol at the MP4/6-31G(d)//MP2/6-31G(d) level). This process would scramble the four deuteriums in **1A-d$_4$**/**1B-d$_4$**. To test this assumption, we prepared the mixture of isotopomers (mono-, di-, tri-, and tetradeuterated) in which deuterium was introduced at the C2 and/or C5 methylene positions. The comparison of the ^{13}C NMR spectra of this mixture and the starting **1A-d$_4$**/**1B-d$_4$** revealed that scrambling of the deuteriums already occurs in the starting compound **1A-d$_4$**/**1B-d$_4$**. The four deuteriums were statistically distributed only on four C atoms (at C2, C5, C1, and C1′), while under our experimental conditions there were no noticeable deuterium content on carbons C3 and C4. The lack of the complete scrambling of the deuteriums at the cyclopentyl ring of **1A**/**1B**, which presumably occurs by a series of 1,2-hydride shifts, is due to the fact that the barrier for the hydride migration from the C2 to C3 carbon atom is much higher (for ca. 7 kcal/mol at

the B3LYP/6-31G(d) level) than for the hydride migration from the C1 to C2 carbon atom. This is in accord with the experimental findings of Forsyth,[13] who showed that the hydride migration on the cyclopentyl ring in the tetradeuterated 1-methyl-1-cyclopentyl cation occurs at temperature above −80 °C and is slow on the NMR time scale.

According to quantum chemical calculations, pathways II and III proceed through almost the same barrier. Since both rearrangements start from the same more stable isomer **1B**, a mixed mechanism would be expected. Advantage can be taken of the large difference in KIEs predicted for rearrangement of the hexadeuterated isotopomer **1A-d_6**/**1B-d_6** (2.24 for pathway II vs 0.89 for pathway III), and the fraction of a certain route in the overall rearrangement can be estimated. A greater fraction of the reaction that proceeding through pathway III would cause a greater decrease of KIE predicted for pathway II. Surprisingly, the experimental KIE for the hexadeuterated compound is not decreased at all (Table 2), indicating that the fraction of the reaction that proceeds through route III is negligible. This can be due to the fact that electron correlation effects considered by the MP2 method favor the bridged structures to a great extent.[14] In **TS-III** bridging is much more pronounced than in **TS-II**, so the actual barrier for pathway III is likely to be larger than the calculated value.

In conclusion, experimental KIEs for the rearrangement of the 2-cyclopentyl-2-propyl cation **1A** and the 1-(2-propyl)cyclopentyl cation **1B** indicate that the major reaction route is that presented as pathway II, which is also calculated (MP4/6-31G(d)//MP2/6-31G(d) level) to be the most favorable. Other two possible routes, pathways I and III, occur probably only as a small fraction of the overall rearrangement process. Nevertheless, in all plausible reaction routes the formation of the secondary six-membered carbocation as an energy minimum is unfavorable, so the reaction proceeds through a highly organized transition state. This conclusion must be true in enzymatic biosynthesis, as well. The origin of stabilization depends on the carbocation structure and its environment. Thus, the remote double bond can participate in the transition state stabilization as was recently suggested by Hess[15] who proposed that in the protosteryl cation the concomitant C-ring expansion and the D-ring cyclization occur. If the double bond is not present in carbocation structure, as is the case with the lupenyl cation (Scheme 1), the bridged transition structures analogous to **TS-I** and **TS-II** may occur. Therefore, formation of taraxasteryl cation from the lupenyl cation (Scheme 1) is likely to proceed according to Pathway II. However, some phytosterol structures could be derived only from the secondary cation intermediate. For example, the structure of the β-amyrin can be rationalized only if the secondary oleanyl cation is considered as an intermediate. Stabilization of such cations in enzymatic conditions probably come from external interactions with π-electrons of aromatic amino acid residues of the enzyme.[16]

Methods

Computational Details. All structures were fully optimized (in the specified symmetry) using the DFT-hybrid and Möller−Plesset perturbation theory. The B3LYP functional was used, which combines Becke's three-parameter exchange functional with the correlation functional of Lee, Yang, and Parr.[17] The ab initio calculations were performed using frozen core (FC) second-order MP2 perturbation correction and fourth-order MP4(SDTQ) theory with single, double, triple, and quadruple substitutions.[18]

The standard split valence and polarized 6-31G(d) basis set was employed in the geometry optimizations and frequency calculations. A vibrational analysis was performed at the same level of theory in order to determine the zero-point vibrational energy (ZPE) and to characterize each stationary point as a minimum (NImag = 0) or transition state structure (NImag = 1). A more complete treatment of electron correlation was made by performing MP4(SDTQ)/6-31G(d) single-point energy calculations for the MP2/6-31G(d)-optimized structures; thus our final level is MP4(SDTQ)/6-31G(d)//MP2/6-31G(d). The inclusion of MP4 correlation energy correction is necessary to correctly estimate the relative energy differences for carbocations involved in the processes under study.[4] Corrections for ZPE (not scaled) are included in the calculated energies.

IRC calculations (intrinsic reaction coordinate as implemented in Gaussian 94) were performed at the B3LYP/6-31G(d). The initial geometries used were that of the corresponding transition states (**TS-I**, **TS-II**, **TS-III**), and the paths were followed in both directions from that point. This method verified that a given transition structure indeed connects the presumed energy minimum structures.[19]

Sample Preparation. The tertiary alcohols **1A-OH** or **1B-OH**, **1B-d_6-OH**, **1A-d_4-OH**, **2A-OH** or **2B-OH**, **2B-d_6-OH**, and **2A-d_4-OH** and partially deuterated isotopomers, which were used as a precursors for the carbocations, were prepared by standard Grignard reaction, as described earlier.[4] Carbocations and their isotopomers were prepared from the corresponding alcohols with excess SbF_5 and a mixture of $SO_2ClF-SO_2F_2$ as solvent, using contemporary high vacuum, co-condensation matrix techniques.[20]

Kinetic Measurements. Ring-expansion rates were followed using solutions of the carbocations. The solutions were prepared from the corresponding alcohols (95 mg) with excess SbF_5 (0.6 mL) and a 2:1 mixture of SO_2F_2/SO_2ClF (3.4 mL) as a solvent. Routine ^{1}H NMR spectra (400 MHz) were run at selected temperatures. The internal standard tetramethylammonium fluoride (10 mg) was used (singlet at 3.0 ppm).

In the rearrangement process of the protio (**1A**/**1B**) and tetradeuterated isotopomers (**1A-d_4**/**1B-d_4**) the disappearance of the of the methyl signals at 2.2 ppm and the concomitant appearance of the methyl signals at 2.5 ppm in the rearranged cation **2** were monitored by recording the spectra at given time intervals. In the case of the hexadeuterated isomer **1A-d_6**/**1B-d_6**, the disappearance of the ring methylene protons on carbons 2 and 5 in **1A-d_6**/**1B-d_6** (at 4.9 ppm) and the appearance of the methylene protons at carbon C2 and C5 in the rearranged cation **2** (at 4.6 ppm) were followed.

(13) Botkin, J. H.; Forsyth, D. A.; Sardella, D. J. *J. Am. Chem. Soc.* **1986**, *108*, 2797.
(14) (a) Schleyer, P. v. R.; Maerker, C. *Pure Appl. Chem.* **1995**, *67*, 755. (b) Schleyer, P. v. R.; Maerker, C.; Buzek, P.; Sieber, S. Accurate Carbocation Structure: Verification of Computed Geometries by NMR, IR, and X-ray Diffraction. In *Stable Carbocations*; Prakash, G. K. S., Schleyer, P. v. R., Eds.; Wiley: New York, 1997.
(15) Hess, B. A., Jr. *J. Am. Chem. Soc* **2002**, *124*, 10286.
(16) (a) Dougherty, D. A. *Science* **1996**, *271*, 163. (b) Miklis, P. C.; Ditchfield, R, Spencer, T. A. *J. Am. Chem. Soc.* **1998**, *120*, 10482. (c) Pale-Grosdemange, C.; Feil, C.; Rohmer, M.; Poralla, K. *Angew. Chem.* **1998**, *110*, 2355.
(17) Lee, C.; Yang, W.; Parr, R. G. *Phys. Rev. B* **1988**, *37*, 785.
(18) Krishnan, R.; Frisch, M. J.; Pople, J. A. *J. Chem. Phys.* **1980**, *72*, 4244.
(19) Gonzalez, C.; Schlegel, H. B. *J. Phys. Chem.* **1990**, *94*, 5523.
(20) Lenoir, D.; Siehl, H.-U. *Houben-Weyl: Methoden der Organischen Chemie*; Georg Thieme: Stuttgart, 1990; Vol. E19C, p 26.

Acknowledgment. We gratefully acknowledge the financial support of this research by the National Science Foundation (Grant No. 0120505) and the Ministry of Science and Technology of the Republic of Croatia (Grant No. 0006451). We thank Prof. H.-U. Siehl (University of Ulm) who enabled us to perform a part of the experimental work in his laboratory.

Supporting Information Available: *xyz* coordinates, total energies (*E*), zero-point energies (ZPE), and number of imaginary frequencies (NImag) calculated for structures **1A**, **1B**, **2**, **2TS**, **3**, **3TS**, **4**, **4TS**, **TS-I**, **TS-II** and **TS-III**. This material is available free of charge via the Internet at http://pubs.acs.org.

JO020694P